

Reconstruction incorporated respiratory motion correction in clinical simultaneous PET/MR imaging for oncology applications

Hadi Fayad¹, Holger Schmidt², Christian Wuerslin², Dimitris Visvikis¹

¹ INSERM, UMR1101, LaTIM, CHRU Morvan, Université de Bretagne Occidentale Brest, France

² University Hospital of Tübingen, Tübingen, Germany

Corresponding author:

FAYAD Hadi

LaTIM, INSERM UMR1101,

CHRU Morvan, 2 avenue Foch,

29609 Brest Cedex, France

Tél: +33 (0) 298-018-111

Fax: +33 (0) 298-018-124

Email: fayad@univ-brest.fr

Short running title: Motion correction in clinical PET/MR

ABSTRACT

Simultaneous positron emission tomography (PET) and magnetic resonance imaging (MRI) is a promising new technique allowing the fusion of functional (PET) and anatomical/functional (MR) information. In the thoracic-abdominal regions, respiratory motion is a major challenge leading to reduced quantitative and qualitative image accuracy. Correction methodologies include the use of gated frames which lead to low signal to noise ratio (SNR) considering the associated low statistics. More advanced correction approaches, previously developed in PET/Computed Tomography (CT) imaging, consist on either registering all the reconstructed gated frames to the reference one or incorporating motion parameters into the iterative reconstruction process to produce a single motion-compensated PET image. The goal of this work was to compare these two, previously implemented in PET/CT, correction approaches within the context of PET/MR motion correction for oncology applications using clinical 4D-PET/MR acquisitions. Two different correction approaches were evaluated, comparing the incorporation of elastic transformations extracted from four dimensional (4D) MRI datasets during PET list-mode image reconstruction to a post-reconstruction image based approach. **Methods:** Eleven patient datasets acquired on the SIEMENS mMR PET/MR system were used. T1-weighted 4D-MR images were registered to the end expiration image using a non-rigid B-spline registration algorithm to derive deformation matrices (DMs) accounting for respiratory motion. The derived matrices were subsequently incorporated within a PET image reconstruction of the original emission list-mode data (reconstruction space (RS) method). The corrected images were compared with those produced by applying the DMs in the image space (IS method) followed by summing the realigned gated frames, as well as with uncorrected motion averaged images. **Results:** Both correction techniques lead to significant improvement in accounting for respiratory motion artifacts when compared to uncorrected motion average images. These improvements include SNR (mean increase of 28.0% and 24.2% for the RS and IS methods respectively), the lesion size (reduction

of 60.4% and 47.9% respectively), lesion contrast (increase of 70.1% and 57.2%) and lesion position (changes of 60.9% and 46.7%). **Conclusion:** Our results demonstrate significant respiratory motion compensation using both methods, with superior results from a 4D-PET RS approach.

Keywords: 4D-PET/MRI, reconstruction based, respiratory motion correction.

INTRODUCTION

Simultaneous PET/MR is a promising multimodality imaging technique allowing the fusion of functional (PET) and anatomical/functional (MR) information. In the thoracic-abdominal region, respiratory motion is a major challenge for PET imaging (1-3). Correction methodologies involve the use of gated frames that are of low SNR since each frame contains only part of the counts available in a motion average PET study (4-6). More advanced correction approaches, consist of either accounting for motion in image space (7), where respiratory gated images are deformed to a reference state and summed, or incorporating motion parameters into the iterative image reconstruction process to produce a single motion-compensated PET image (8, 9). Within the context of motion compensation, it has been previously shown that the necessary motion parameters may be extracted directly from the PET images (10). However, this approach is limited by the resolution of the DMs which is equivalent to the PET image resolution (10). Additionally, this approach is likely to fail for specific radiotracers with little background uptake (7), such as for example C-11 acetate imaging. Instead, the DMs can be derived using other modalities, such as 4D-CT in the case of combined PET/CT systems. However, the use of 4D-CT images is hampered by several issues, the most important being the associated dose to the patient (11). In addition, differences between corresponding gated frames in 4D-PET and corresponding phase matched 4D-CT series have been previously reported in PET/CT imaging. Such mismatches are resulting from differences in the conditions of respiratory synchronized PET and CT acquisitions. In turn such differences result in errors associated with the derivation of DMs from 4D-CT frames for PET motion correction (12, 13). In the case of PET/MR systems, these two issues, associated with the use of 4D-CT acquisitions are irrelevant, given the non-ionising nature of MR acquisitions, its good tissue contrast even in the lungs as demonstrated using newly developed algorithms (14), and the capability of simultaneous PET and MR acquisitions.

Recently, the use of simultaneous PET/MR has been proposed for the generation of DMs (15),

initially to correct for rigid head motion in brain imaging (16). In the case of non-rigid respiratory motion, the use of 2-dimensional (2D) and 3-dimensional (3D) MR sequences for non-rigid motion compensation have been proposed and evaluated using simulated PET data (17, 18), phantom studies (19, 20), and in rabbits and primates (21). To our knowledge the only study, for respiratory motion correction in clinical PET/MR imaging using patient datasets was described by Wurslin et al. (22). The proposed method was shown to work well in a time-efficient and convenient manner allowing for easy integration into clinical routine imaging given that the DMs are extracted by acquiring, in a simultaneous fashion during the first 3 minutes of the PET scan, multiple sagittal 2D-MR slices covering the patient's body within the PET field of view (FOV). The rest of the process involves the acquisition of 2D navigators with no associated time implications. On the other hand, this method was a post-reconstruction image based motion correction and therefore results could be potentially improved by integrating DMs within the PET reconstruction (9).

In this work we compare for the first time in clinical simultaneous 4D-PET/MR imaging for oncology applications two different respiratory motion correction implementations, previously considered in the field of 4D-PET/CT. Within this context, the application of DMs extracted from 4D-MR images during PET image reconstruction in order to produce a single motion-compensated PET image was evaluated. The proposed method was compared to the image based correction approach presented in (22).

MATERIALS AND METHODS

Patient Datasets

11 enrolled patients (7 male, 4 female) with metastatic lesions in the thorax or upper abdomen participated in the study (age 32-70 y; mean 57 ± 11 y). Table 1 shows an overview of the patient demographics, including the corresponding lesion characteristics. Patient datasets were

acquired on a hybrid whole-body PET/MR system (Biograph mMR; Siemens Healthcare, Erlangen, Germany). The scanner combines a PET detector system with a transaxial and axial FOV of 59.4 cm and 25.8 cm respectively, and a 3T MR system. Phased-array body coils optimized for minimizing 511-keV photon attenuation were used for MR signal detection. A T1-weighted spoiled gradient-echo sequence with Dixon-based fat-water separation was acquired in breath-hold (echo times 1.23 ms and 2.46 ms, repetition time 3.6 ms, flip angle 10°, resolution 2.6x2.6x2.6 mm, bandwidth 965 Hz/px, parallel imaging acceleration factor 2, 128 slices per slab, acquisition time 19s, end-expiratory position), and tissues were classified to obtain an attenuation map for the entire PET FOV (23). PET emission data of one bed position covering thorax and upper abdomen were subsequently recorded in list mode format for 5 minutes under free breathing conditions. PET/MR scanning started without repeated radiotracer injection after routine whole body PET/CT acquisition (122±13 min after injection of 336–371 MBq of 18F-FDG).

The 1D respiratory signal used for PET data binning was extracted from 2D-MRI navigator images of the diaphragm position (22) acquired throughout the PET data acquisition. During the first 3 minutes of the PET scan, multiple sagittal 2D-MR slices covering the patient's body within the PET FOV were acquired in order to obtain a 4D-MR series (echo time 1.8 ms, repetition time 3.7 ms, flip angle 15°, resolution 2x2x10 mm³, bandwidth 670 Hz/px, 36 slices per slab, 0.4s acquisition time per image slice) and framed into 4 different MR images. This is done by inserting, for each slice, the MR image closest to the frame's mean respiratory position, into the corresponding 3D volume of the four frames. The choice of four frames was based on previous work (22) (Supplemental material fig 3 & 4), where it was shown that for a 5 min PET acquisitions with the mMR system, 4 respiratory gates resulted in superior lesion contrast, SNR, and full width at half maximum (FWHM) results compared to 6/8 gates. All patients provided written informed consent for participation in the 4D-PET/MR study, which was approved by the local institutional review board.

Motion Parameters Extraction

The T1-weighted 4D-MR images were registered to the end expiration image using a non-rigid B-spline registration algorithm (24) to derive DMs accounting for the respiratory motion. The end expiration image was considered as the PET reference frame since it corresponds to the breath-hold state of the MR based attenuation correction acquisition. The elastic registration was performed using a spatio-temporal algorithm for motion reconstruction from a series of images. This method uses a semi-local parametric model for the deformation based on B-splines and reformulates the registration task as a global optimization problem (24). The obtained transformation $U_t(x)$ between the MR image $m(x,t)$ at time t (t can be 1, 2 or 3 corresponding to the three 4D-MR images) and the end expiration MR image $m(x,0)$ is defined as a linear combination of B-spline basis functions, located in a rectangular grid:

$$U_t(x) = x + \sum_{j \in \mathbb{Z}^N} c_j \beta_r \left(\frac{x}{h} - j \right) \quad (1)$$

where, j are the indices of the grid location and β_r is a tensor product of centered B-splines of degree r . The spacing between the grids h determines the number of parameter c_j to be optimized and the solution rigidity. The registration is then formulated as an optimization procedure minimizing the sum of squared differences metric to find the best transformation parameter c_j (25). To improve speed and robustness, a multi-resolution approach is used in the image and the transformation space (24). This approach creates a pyramid of subsampled images optimal in the L2-sense taking advantage of the spline representation. The problem is solved starting at the coarser to the finest level.

PET Image Reconstruction Based Respiratory Motion Correction

Before sorting the list-mode data into respiratory gates, the data was synchronized with the MR-derived respiration signal by parsing the list-mode data file using a synchronization tag that is

inserted by the MR scanner at the beginning of the imaging sequence. The MR navigator data were acquired during the full PET acquisition and were used to define 4 respiratory gates with respect to the diaphragm motion amplitude and hence corresponding to the 4 previously mentioned 3D-MR frames.

A list mode based respiratory motion correction was implemented during PET image reconstruction, allowing the use of all acquired data available throughout a respiratory motion average acquisition. The elastic DMs, extracted as described in the previous section were incorporated within the one-pass list mode expectation maximization (OPL-EM) algorithm to reconstruct a single motion-compensated PET image, according to a previously validated implementation (9).

The standard OPL-EM algorithm can be written as follows:

$$n_j^{k+1} = n_j^k \sum_{i \in T^k} p_{ij} \frac{1}{q_i^k} \quad \text{for } k=1, \dots, K \quad (2)$$

where, $q_i^k = \sum_{j=1}^J p_{ij} n_j^k$ is the expected count in line of response (LOR) i , p_{ij} is the purely geometric term representing the geometric probability of detecting at LOR i an event generated in voxel j , n_j is the voxel j intensity, J is the total number of voxels, s_j is the voxel j of the sensitivity image and K is the number of time subsets k . k is both the iteration number and the number of subset used in that iteration. T^k is the set of list mode events in the k^{th} subset. The sensitivity image S including the normalization and attenuation corrections is produced through a forward-projection and back-projection of the attenuation image (9).

The discrete motion DMs u_t (calculated in equation 1) can be incorporated in a mathematical representation of the system matrix in the PET reconstruction process (9). If P is the system matrix, whose elements p_{ij} represent the geometric probability of detecting at LOR i an event generated in voxel j (equation 2), the new motion compensation incorporated system matrix P_t accounting for the deformation of the radioactive distribution from time t to the reference time

using matrix u_t can be described as follows:

$$P_t = P.u_t \quad (3)$$

The standard OPL-EM algorithm (equation 2) is subsequently modified to:

$$n^{k+1} = \frac{n^k}{s} \sum_{N_{frames}} P_t^T \frac{1}{P_t n^k} \text{ for } k= 1, \dots, K \quad (4)$$

where, T is the transpose operator and N_{frames} (4 in this study) is the number of temporal gated frames (number of DMs+1). The sensitivity image S used for attenuation and normalization correction was also modified to account for the motion of the voxel location by using the modified system matrix P_t (9).

Image Analysis and Validation

The accuracy of the proposed RS correction method described above was assessed by comparing the single motion-compensated PET image produced using this approach (RS motion corrected PET image, "RSC-image"), with the one produced by applying the elastic transformations in the IS followed by summing together the realigned gated frames (IS corrected image, "ISC-image"). In addition, the uncorrected motion average image ("NC-image") was considered for comparison purposes.

Local profiles were used as qualitative figures of merit. The first chosen quantitative figure of merit was the difference in SNR in a uniform activity distribution organ between corrected and motion average PET images. The SNR is defined as the power ratio between a signal (in the liver) and the background noise. The signal is calculated by using the mean of ten circular regions of interest (ROIs) of 3cm in diameter covering the whole of the liver. The background noise was given by the standard deviation in these ROIs. The second quantitative figure of merit was the percentage improvement of the lesion contrast calculated using a similar ROI analysis. Ten ROIs of 3cm in diameter were placed in the background organ where each lesion was located. The mean activity concentration in these background ROIs was used in the lesion to

background contrast calculations. The slice with the maximum count density over the lesion was identified for the ROIs analysis. Average count densities were subsequently derived for the lesion.

Finally, other quantitative figures of merit considered were the lesion position and size (in terms of FWHM changes). In order to assess the effects on both the lesion location and size, line profiles were obtained for each lesion. Each of the lesion profiles was subsequently fitted with a Gaussian function in order to derive the lesion position and corresponding lesion size (FWHM). Finally the percentage improvement for all quantitative figures of merit was calculated using the following equation:

$$\%improvement = \left| \frac{X_{Corrected} - X_{Non-Corrected}}{X_{Non-Corrected}} \right| \times 100 \quad (4)$$

where, X is either the lesion contrast, position or FWHM, the corrected image may be either the “RSC-image” or the “ISC-image”, and the non-corrected image is the “NC-image”. Finally, the results of the correction methods were statistically compared using the Wilcoxon two-sample paired signed rank test (MedCalc software, Belgium). P values below 0.05 were considered significant.

RESULTS

Figure 1.A, B and C show the “RSC-image”, the “ISC-image” and the “NC-image”, respectively. Profiles along the lesion for one patient (figure 1.D) indicate high correlation between the two methods with a noticeable difference compared to the “NC-image”. In particular the tumor on the “NC-image” displays different activity distribution heterogeneity patterns relative to the motion corrected images.

Considering the quantitative figures of merit, the SNR indicates an improvement of $28.0 \pm 5.3\%$ for the “RSC-image” in comparison to $24.2 \pm 6.0\%$ in the case of the “ISC-image” relative to the “NC-image”. In terms of contrast improvements, figure 2 shows a mean contrast increase of

70.1±27.9% and 57.2±20.2% for the “RSC-image” and the “ISC-image” respectively. This difference was significant between the two correction methods when using the Wilcoxon rank sum test ($p=0.001$). Considering the lesion position results, shown in figure 3.A, average differences in position percentage change of 60.9±21.7% and 46.7±22.4% for the “RSC-image” and the “ISC-image” respectively were found, indicating that both motion correction methodologies lead to changes compared to the “NC-image” with a statistically significant advantage ($p=0.002$) for the RS vs the IS based motion correction. The corresponding position change in mm (figure 3.B) was 9.04±3.27mm vs 7.74±2.99mm respectively. Finally, the lesion FWHM also showed statistically significant differences when using the RS based motion correction ($p=0.001$, when comparing the two correction methods) with a mean lesion FWHM reduction of 60.4±21.0% and 47.9±16.2% for the “RSC-image” and the “ISC-image” respectively.

DISCUSSION

The goal of this work was to demonstrate the feasibility of image reconstruction incorporated respiratory motion correction in clinical PET/MR in comparison with an image based correction approach. The RS method was based on the application of DMs extracted from 4D-MRI datasets to the list-mode data during image reconstruction. The second approach was based on applying the 4D-MRI DMs directly on the reconstructed respiratory synchronized PET images. Eleven patient datasets acquired on a dedicated simultaneous PET/MR imaging system were included in the validation stage. Results demonstrate that both techniques lead to significant improvements in correcting for respiratory motion artifacts when compared to NC images. Moreover, the RS correction led to overall superior SNR and lesion contrast, with reduced lesion sizes when compared to the equivalent IS correction. As shown in our results, the magnitude of the motion correction effect was more important for patient lesions with large motion, especially those located on the lower lobe of the lungs or in the spleen.

This RS approach was originally proposed and evaluated in 4D-PET/CT imaging (8, 9, 26, 27).

In the current study we show its applicability to clinical 4D-PET/MR imaging and demonstrate its advantages relative to the IS method. This was confirmed by the mean lesion contrast improvement (+12.9%), changes in mean lesion position (14.2%) and lesion FWHM (12.5%). These patient results are in accordance with those obtained in 4D-PET/CT using simulated images (9, 28). Lamare et al. (9) showed an increased lesion contrast (20%-30%) as a result of using the RS motion correction compared to the IS correction. Within the same study, they showed also improvements of >10% in magnitude on recovered lesion position and size between the two motion correction implementations. On a theoretical study using simulated datasets for thoracic PET/CT imaging, Polycarpou et al. showed a superior performance for the RS motion correction in terms of activity concentration recovery accuracy relative to the IS correction (28). The advantages of the RS motion compensation are due to multiple factors. Firstly, the IS correction suffers from the low count statistics associated with each synchronized frame which may cause convergence related biases in the resulting gated reconstructed images. Furthermore, the image registration step of the individual gated PET frames that follows may introduce interpolation effects into the final image leading to resolution degradation and potential artifacts. Although such transformations are also used during the RS motion correction, these are not applied directly to the images but during the forward and back-projection steps which could minimize errors (29). Finally, in terms of computational cost the two correction implementation are practically equivalent. On the other hand, one has to consider the easiness of implementation for the IS approach as well as the need and added complexity of accurately accounting for attenuation and/or scatter corrections within the context of the RS motion correction.

A possible extension of the present study would be the comparison of DMs derived from 4D-MR and 4D-CT acquisitions on the same patient population. Although this was not the case in our patient cohort, if for each patient both 4D-CT and 4D-MR images were available the influence of the 4D anatomical image series used to derive the DMs to the RS or IS motion compensation

performance would have been possible. Since 4D-CT and corresponding 4D-MR images would have different characteristics in terms of tissue contrast but also as a result of differences in data acquisition and associated sorting methodologies, one may expect the use of different image registration parameters and associated motion information extraction. On the other hand, the impact of such potential differences may be limited if one considers a combination of the overall respiratory motion amplitude and the limited spatial resolution of the PET images we are seeking to correct.

A possible limitation of this study is the relatively small numbers of patients. Additional patients may further enhance the differences in the performance of the two correction methodologies tested in this study. However, the results based on the use of eleven PET/MR patient datasets seem conclusive with respect to the potential impact of respiratory motion correction in PET/MR for oncology applications.

Another limitation of this PET/MR study is the use of a 2 point Dixon's approach for attenuation correction (acquisition time of 19s), by classifying tissues into four different classes (air, lung, soft tissue, and adipose tissue), without any bone structures consideration. To resolve this issue, an ultra-short echo-time triple-echo (UTILE) MRI sequence (acquisition time of 100s) may be used (30), combining UTE sampling for bone detection and gradient echoes for Dixon water-fat separation in a radial 3-dimensional acquisition. Since the attenuation correction data acquisition is carried out during breath hold while the PET data is acquired under free breathing, an intrinsic mismatch may occur between the end-expiratory attenuation map and the end-expiratory state of the 4D-MR motion data. Thus, creating a motion-corrected attenuation map directly from the 4D-MR data, used for determining the patient motion, might be more appropriate.

In this work, the overall MR sequence acquisition associated with the motion correction task was 3 minutes long. A possible extension of the proposed correction methodology may be based on integrating a previously proposed respiratory motion model (31) in order to improve the temporal resolution (number of DMs) of the DMs used in the correction process (3 in this study). This can

be done, as shown in preliminary results (32), by creating a motion model based on a relationship between a 2D-MR navigator and the 3D motion field allowing the generation of 3D-MR volumes and their corresponding DMs for each temporally corresponding navigator. In order to build such a model, a number (10-15) of patient 4D-MR image datasets and corresponding 2D navigators are needed. However once the model is built, for a new patient only 2D navigator acquisitions in parallel to the PET data acquisition would be needed, without increasing overall acquisition times. An alternative solution will be the use of existing or the development of new approaches allowing 4D-MR sequences acceleration (33) leading to the availability of 4D-MR datasets with higher temporal and/or spatial resolution without further increasing overall acquisition times. These datasets can be used to improve the accuracy and temporal sampling of the DMs used in the RS PET motion compensation scheme proposed in this work (34).

CONCLUSIONS

A list-mode reconstruction based respiratory motion correction for PET has been implemented and its performance evaluated on clinical 4D-PET/MR patient datasets. This approach was based on the use of elastic transformations derived from 4D-MRI during PET image reconstruction. Our results show significant respiratory motion compensation when compared to the motion average PET images, with improved SNR, lesion contrast and reduced lesion size compared to an equivalent 4D-PET IS elastic motion correction method.

ACKNOWLEDGMENTS

This study was partly financially supported by the EU COST action TD1007 (www.pet-mri.eu).

References

1. van Elmpt W, Hamill J, Jones J, De Ruyscher D, Lambin P, Ollers M. Optimal gating compared to 3D and 4D PET reconstruction for characterization of lung tumours. *Eur J Nucl Med Mol Imaging*. 2011;38:843-855.
2. Polycarpou I, Tsoumpas C, King AP, Marsden PK. Impact of respiratory motion correction and spatial resolution on lesion detection in PET: a simulation study based on real MR dynamic data. *Phys Med Biol*. 2014;59:697-713.
3. Zaidi H, Del Guerra A. An outlook on future design of hybrid PET/MRI systems. *Med Phys*. 2011;38:5667-5689.
4. Bruyant P, Turzo A, Bizais Y, Cheze Le Rest C, Visvikis D. A comparison of three respiratory gating methods in PET imaging for oncology. *J Nucl Med*. 2006;47:1.
5. Nehmeh SA, Erdi YE. Respiratory motion in positron emission tomography/computed tomography: a review. *Semin Nucl Med*. 2008;38:167-176.
6. Nehmeh SA, Erdi YE, Pan T, et al. Quantitation of respiratory motion during 4D-PET/CT acquisition. *Med Phys*. 2004;31:1333-1338.
7. Dawood M, Lang N, Jiang X, Schafers KP. Lung motion correction on respiratory gated 3-D PET/CT images. *IEEE Trans Med Imaging*. 2006;25:476-485.
8. Lamare F, Cresson T, Savean J, Cheze Le Rest C, Reader AJ, Visvikis D. Respiratory motion correction for PET oncology applications using affine transformation of list mode data. *Phys Med Biol*. 2007;52:121-140.
9. Lamare F, Ledesma Carbayo MJ, Cresson T, et al. List-mode-based reconstruction for respiratory motion correction in PET using non-rigid body transformations. *Phys Med Biol*. 2007;52:5187-5204.
10. Lustig M, Donoho D, Pauly JM. Sparse MRI: The application of compressed sensing for rapid MR imaging. *Magn Reson Med*. 2007;58:1182-1195.
11. Beyer T, Townsend DW, Brun T, et al. A combined PET/CT scanner for clinical oncology. *J Nucl Med*. 2000;41:1369-1379.
12. Fayad HJ, Lamare F, Le Rest CC, Bettinardi V, Visvikis D. Generation of 4-dimensional CT images based on 4-dimensional PET-derived motion fields. *J Nucl Med*. 2013;54:631-638.
13. Goerres GW, Burger C, Schwitter MR, Heidelberg TN, Seifert B, von Schulthess GK. PET/CT of the abdomen: optimizing the patient breathing pattern. *Eur Radiol*. 2003;13:734-739.
14. Baumgartner CF, Kolbitsch C, Balfour DR, et al. High-resolution dynamic MR imaging of the thorax for respiratory motion correction of PET using groupwise manifold alignment. *Med*

Image Anal. 2014;18:939-952.

15. Pichler BJ, Kolb A, Nagele T, Schlemmer HP. PET/MRI: paving the way for the next generation of clinical multimodality imaging applications. *J Nucl Med.* 2010;51:333-336.
16. Catana C, Benner T, van der Kouwe A, et al. MRI-assisted PET motion correction for neurologic studies in an integrated MR-PET scanner. *J Nucl Med.* 2011;52:154-161.
17. Dikaios N, Izquierdo-Garcia D, Graves MJ, Mani V, Fayad ZA, Fryer TD. MRI-based motion correction of thoracic PET: initial comparison of acquisition protocols and correction strategies suitable for simultaneous PET/MRI systems. *Eur Radiol.* 2012;22:439-446.
18. King AP, Buerger C, Tsoumpas C, Marsden PK, Schaeffter T. Thoracic respiratory motion estimation from MRI using a statistical model and a 2-D image navigator. *Med Image Anal.* 2012;16:252-264.
19. Guerin B, Cho S, Chun SY, et al. Nonrigid PET motion compensation in the lower abdomen using simultaneous tagged-MRI and PET imaging. *Med Phys.* 2011;38:3025-3038.
20. Tsoumpas C, Mackewn JE, Halsted P, et al. Simultaneous PET-MR acquisition and MR-derived motion fields for correction of non-rigid motion in PET. *Ann Nucl Med.* 2010;24:745-750.
21. Chun SY, Reese TG, Ouyang J, et al. MRI-based nonrigid motion correction in simultaneous PET/MRI. *J Nucl Med.* 2012;53:1284-1291.
22. Wurslin C, Schmidt H, Martirosian P, et al. Respiratory motion correction in oncologic PET using T1-weighted MR imaging on a simultaneous whole-body PET/MR system. *J Nucl Med.* 2013;54:464-471.
23. Martinez-Moller A, Souvatzoglou M, Delso G, et al. Tissue classification as a potential approach for attenuation correction in whole-body PET/MRI: evaluation with PET/CT data. *J Nucl Med.* 2009;50:520-526.
24. Ledesma-Carbayo MJ, Mahia-Casado P, Santos A, Perez-David E, Garcia-Fernandez MA, Desco M. Cardiac motion analysis from ultrasound sequences using nonrigid registration: validation against Doppler tissue velocity. *Ultrasound Med Biol.* 2006;32:483-490.
25. Sorzano CO, Thevenaz P, Unser M. Elastic registration of biological images using vector-spline regularization. *IEEE Trans Biomed Eng.* 2005;52:652-663.
26. Li T, Thorndyke B, Schreiber E, Yang Y, Xing L. Model-based image reconstruction for four-dimensional PET. *Med Phys.* 2006;33:1288-1298.
27. Qiao F, Pan T, Clark JW, Jr., Mawlawi OR. A motion-incorporated reconstruction method for gated PET studies. *Phys Med Biol.* 2006;51:3769-3783.

28. Polycarpou I, Tsoumpas C, Marsden PK. Analysis and comparison of two methods for motion correction in PET imaging. *Med Phys*. 2012;39:6474-6483.
29. Dikaios N, Fryer TD. Improved motion-compensated image reconstruction for PET using sensitivity correction per respiratory gate and an approximate tube-of-response backprojector. *Med Phys*. 2011;38(9):4958-70.
30. Berker Y, Franke J, Salomon A, et al. MRI-based attenuation correction for hybrid PET/MRI systems: a 4-class tissue segmentation technique using a combined ultrashort-echo-time/Dixon MRI sequence. *J Nucl Med*. 2012;53:796-804.
31. Fayad H, Pan T, Pradier O, Visvikis D. Patient specific respiratory motion modeling using a 3D patient's external surface. *Med Phys*. 2012;39:3386-3395.
32. Fayad HJ, Buerger C, Tsoumpas C, Cheze-Le-Rest C, Visvikis D. A generic respiratory motion model based on 4D MRI imaging and 2D image navigators. Paper presented at: Nuclear Science Symposium and Medical Imaging Conference (NSS/MIC), 2012 IEEE; Oct. 27 2012-Nov. 3 2012, 2012.
33. Odille F, Vuissoz PA, Marie PY, Felblinger J. Generalized reconstruction by inversion of coupled systems (GRICS) applied to free-breathing MRI. *Magn Reson Med*. 2008;60:146-157.
34. Fayad F, Odille F, Schmidt H, et al. The use of a generalized reconstruction by inversion of coupled systems (GRICS) approach for generic respiratory motion correction in PET/MR imaging. *Phys Med Biol*. 2015; 21; 60(6):2529-46.

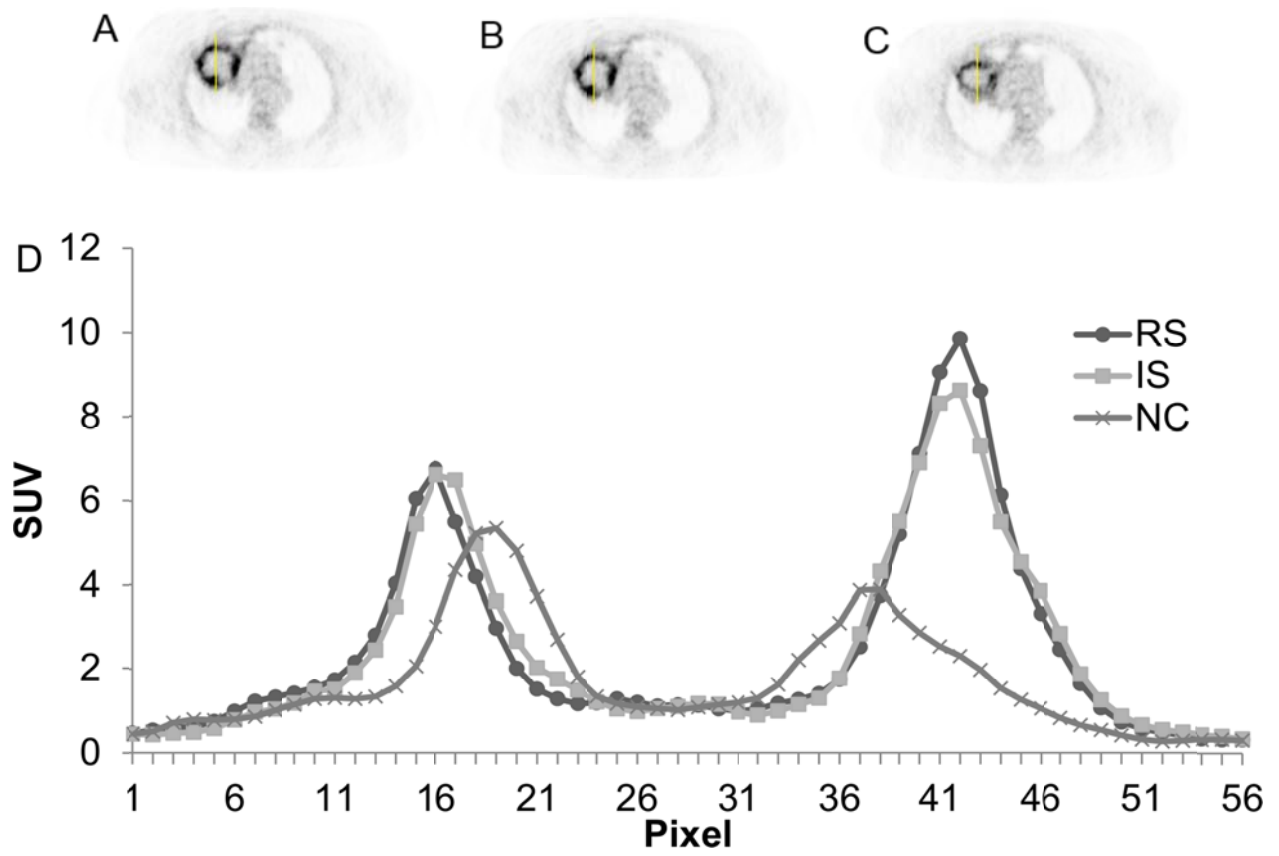


Figure 1: (A) RS motion corrected PET image (B) IS corrected image (C) NC image (D) Corresponding profile

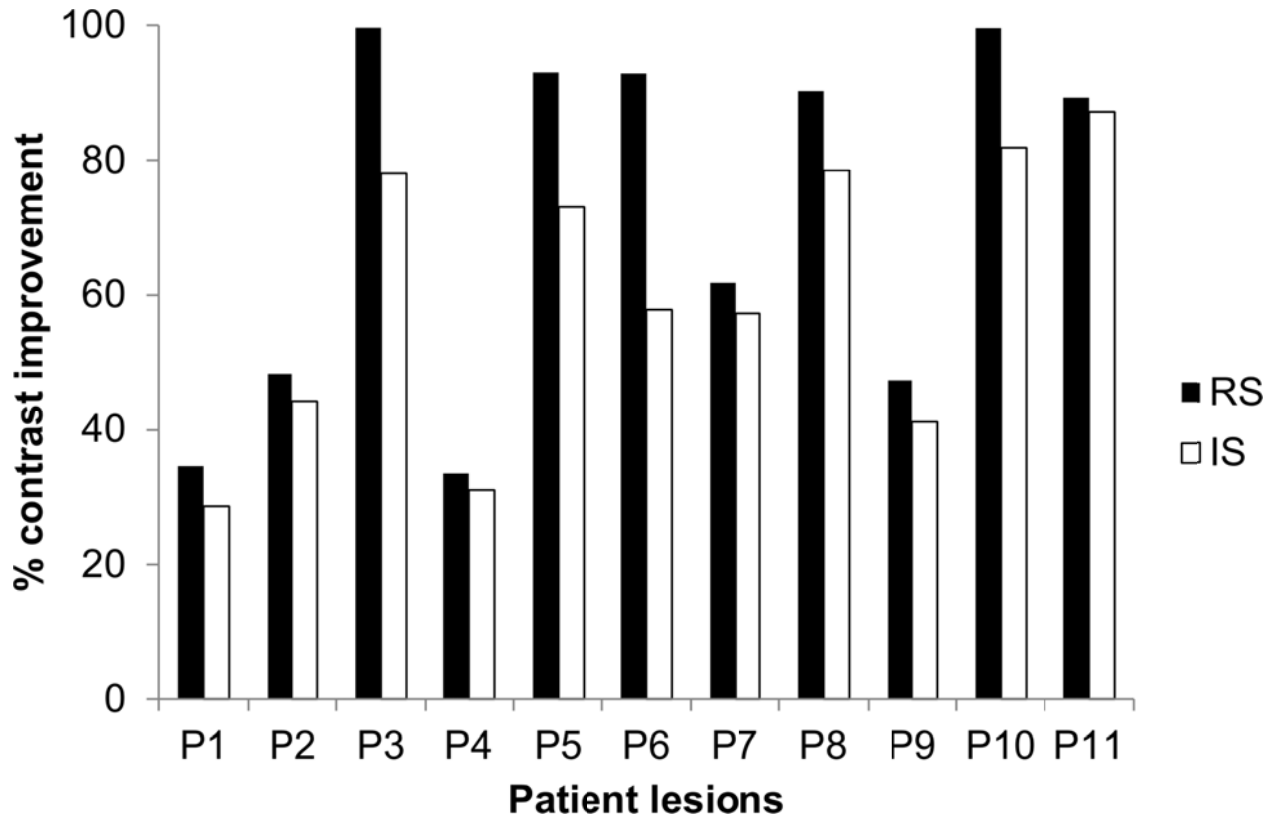


Figure 2: Mean percentage improvement of the contrast of lesions for 11 different patients. Results are shown for both correction approaches; the RS and the IS in comparison to the NC image.

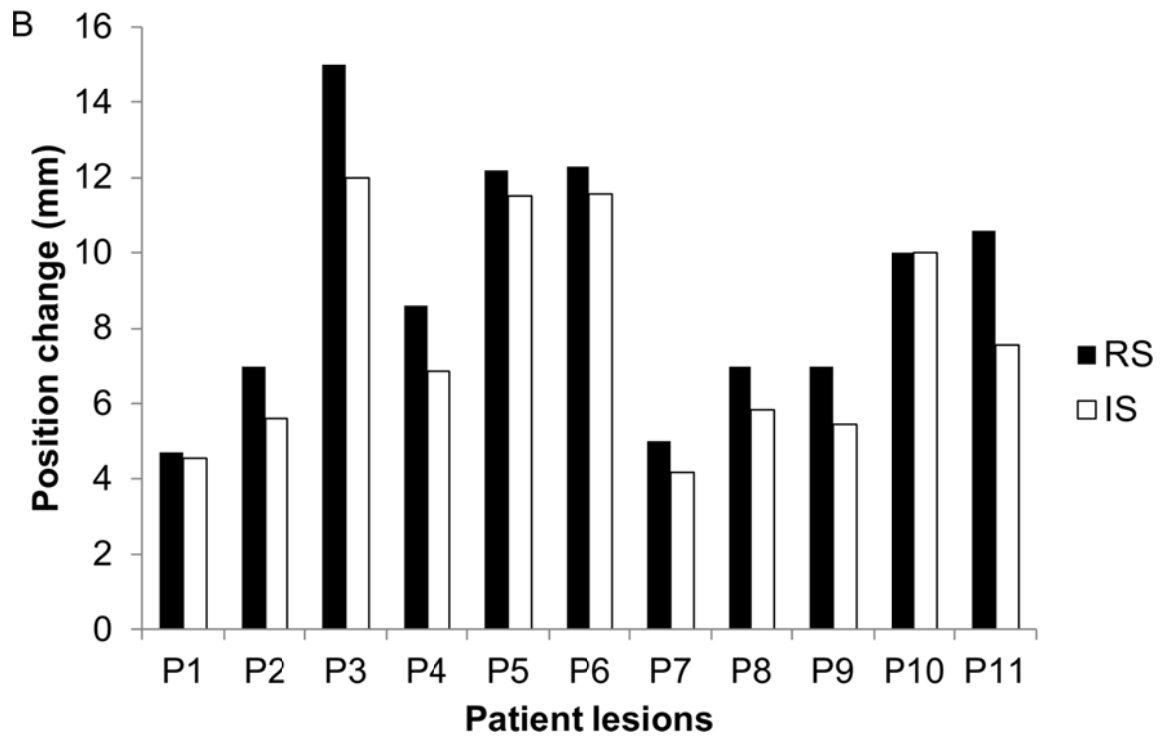
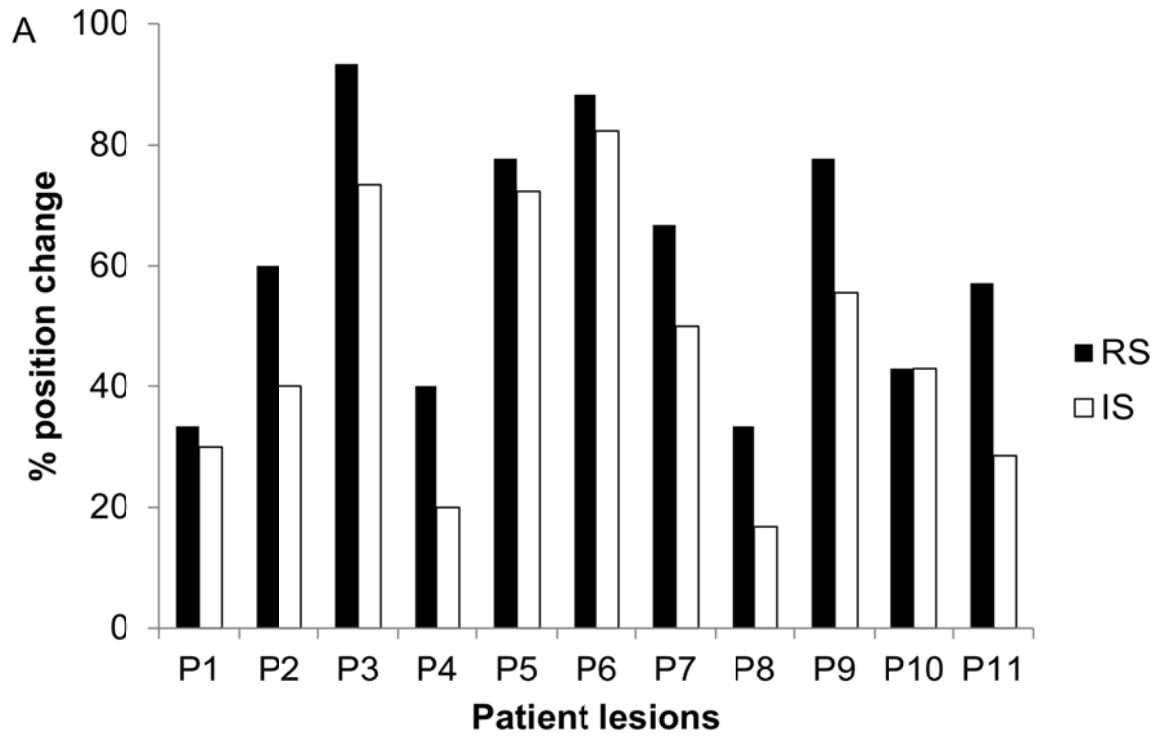


Figure 3: (A) Mean percentage change of the position of lesions for 11 different patients. Results are shown for both correction approaches; the RS and the IS in comparison to the NC image (B) Corresponding change in mm.

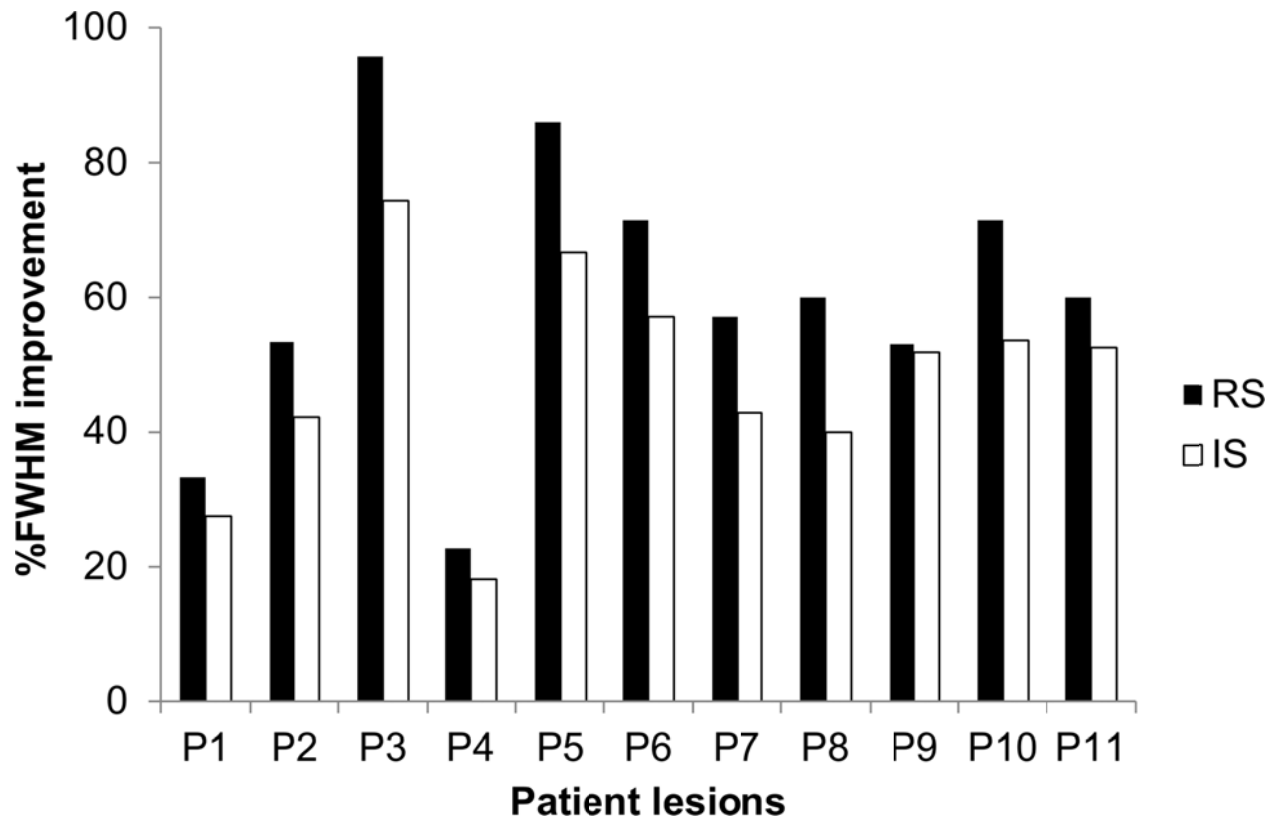


Figure 4: Mean percentage improvement of the FWHM of lesions for 11 different patients. Results are shown for both correction approaches; the RS and the IS in comparison to the NC image.

Table 1: An overview of the patient demographics, including lesion and associated motion characteristics.

Patient	Age (y)	Sex	Type of malignancy	Lesion location	Size (mm ²)*	Lesion displacement (mm)*
P1	67	M	Bronchial carcinoma	Lymph node, hilar	11×10	5.1
P2	61	M	Gastrointestinal stromal tumor	Stomach	12×14	7.4
P3	70	M	Bronchial carcinoma	Lung, lower lobe	13×12	16.2
P4	56	M	Nasopharyngeal carcinoma	Spleen	9×8	9.3
P5	32	F	Sigma carcinoma	Spleen	21×16	13.7
P6	69	M	Bronchial carcinoma	Lung, lower lobe	13×7	13.5
P7	62	F	Laryngeal carcinoma	Lung, middle lobe	8×7	5.6
P8	60	F	Bronchial carcinoma	Lung, lower lobe	13×8	7.4
P9	49	M	esophageal carcinoma	Middle thoracic esophagus	11×8	7.8
P10	54	M	Bronchial carcinoma	Lung, lower lobe	8×8	10.4
P11	52	F	Sigma carcinoma	Lung, lower lobe	8×5	11

* Determined from 4D-MR images